J. Indian Inst. Sci., Sept.–Oct. 2006, **86**, 415–437

Automation of minimum torque-based accurate solar tracking systems using microprocessors

ANAND M. SHARAN* AND MANISH PRATEEK
Faculty of Engineering, Memorial University of Newfoundland, St John's, Newfoundland, Canada A1B 3X5.
email: asharan@engr.mun.ca; Phone: 709-737-8930; Fax: 709-737-4042.

Received on December 24, 2005; Revised on October 13, 2006.

Abstract

In this paper, the dynamic equations for the planetary motion are derived. These are based on the three-dimensional kinematic equations needed for tracking spherical bodies such as the Earth. To track the Sun with minimum torque where the solar energy conversion is maximum, i.e. all the while, the solar rays are incident normal to the receiving surface (the solar panel). The tracking system is designed in such a way that one can track the Sun with the minimum torque. Minimum condition (the minimum torque) is maintained even when the seasonal variation is given to the solar panel frame.

Three methods are discussed here for an automatic operation of the system which includes an intelligent tracking method, in the case of interrupted power supply. This work also introduces microprocessors to track the Sun besides other electronic methods. Accurate tracking takes into account the change in the orientation of the Earth's axis due to the gravitational pull of Jupiter, and the moon.

Keywords: Solar tracking systems, microprocessors, automation, dynamic equations, and planetary motion.

1. Introduction and literature survey

Solar energy systems have become important alternative solutions to environmental problems faced by the world today. The combustion of fossil fuels causes respiratory problems and the humanity will face energy shortage in the not too distant future [1]. Hence, it is rather tempting to exploit solar energy, which is available in abundance, in a practical and optimal manner.

There are two types of systems which utilize solar energy: The first one is the concentrating type, and the other without concentration. The flat plate or photovoltaic panels belong to the latter type, whereas the paraboloidal mirrors belong to the former. In either of the two cases, one enhances the efficiency of the system by tracking. The devices that track the solar position can be of two types; the first utilizes matched solar cells or other photoelectric sensors which generate a differential signal whenever the orientation of the device is not optimal. This signal is used in the feedback mechanism to reorient the receiver until the best orientation is achieved [2–4]. Such devices have not proved to be very reliable as they fail to discriminate between the obscured Sun and a bright spot in a broken cloud. The

*Author for correspondence.

feedback mechanism disorientates the receiver towards the bright spot rather than the Sun. The tracking thus fails. Furthermore, these devices are not dependable under foggy or misty or dusty conditions [5–13]. Agarwal, and Sharan [14] worked on a method of finding an axis in three-dimensional space about which a rotation could be given to track the Sun.

Another type of mechanism which tracks the Sun is the use of clock mechanism to control the orientation of the receiver at different times of the day. Unfortunately, to follow the Sun accurately in its daily as well as yearly (seasonal) motions, the devices have to be complex in their construction besides being expensive to build. In these cases, the torque required varies with the angular orientation of the solar panel. Thus the motor selected has to correspond to the maximum torque requirement amongst all possible orientations of the solar panel. This is in contrast to the present work where the torque is the same and is minimum for all possible orientations.

The disadvantage with both the types of systems mentioned above is the excessive energy requirement during tracking as these are not mass-balanced. Due to the imbalance, far more torque is required to correct the position of the receiver compared to the balanced systems. Many times it is not possible to attain the correct position especially when the Sun appears in the sky after a long interval, owing to cloudy conditions. Under such situations, significant amount of torque is required for the receiver to attain optimal orientation.

The specific contributions of this paper are:

(1) The derivation of the required three-dimensional equations for tracking. These equations enable one to orient the solar panel directly towards the Sun rather than towards the maximum light intensity direction as done in the case of photosensor-based tracking systems. The latter systems fail to orient correctly under scattered cloudy or dusty conditions which are quite common in the tropical areas. The areas of the Earth in these regions receive enormous amounts of solar energy.
(2) The automated design of the tracking system with a minimum torque minimizes energy consumption for tracking, and also for motor horse power requirements. The tracking system presented here is especially suitable for situations where the forces involved are high such as large-scale paraboloidal concentrators or reflectors. Secondly, for space-tracking applications such as mounting telescopes for planetary or deep space observations, the system presented here will be preferable.
(3) Accurate tracking at much finer intervals than is possible by dc motor-driven tracking systems using feedback sensors at coarser intervals.
(4) Automated tracking even in the case of power interruption conditions.
(5) Automated tracking by taking into account the equation of time which is a lead or lag in starting time at sunrise due to mis-orientation of the Earth's spin axis owing to the pull of Jupiter and the moon.

3. Derivation of three-dimensional kinematic equations for tracking

3.1. *Equations for planetary motion of the Earth*

Figure 1 shows the schematic model of the Earth's trajectory around the Sun. Here, it is acted upon by the Sun's gravitational force. At point A, which is a general point (r, θ) in

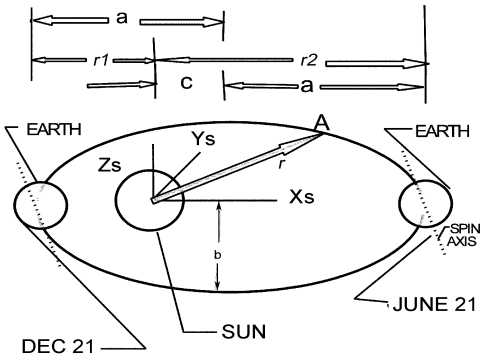

FIG. 1. Earth's orbital motion.

the polar coordinate system, the force equation can be easily derived [15, 16]. These equations along the two polar coordinates are:

$$\sum F_r = -F = m(\ddot{r} - r\dot{\theta}^2), \tag{1}$$

$$\sum F_\theta = 0 = m(r\ddot{\theta} + 2\dot{r}\dot{\theta}), \tag{2}$$

where the magnitude of the centralized force is

$$F = \frac{GMm}{r^2}. \tag{3}$$

Here M is the mass of the Sun, m, the mass of the Earth, and G, the gravitational constant.

We can rewrite eqn (2) as

$$m\frac{1}{r}\left(\frac{\mathrm{d}}{\mathrm{d}t}\left[r^2\frac{d\theta}{dt}\right]\right) = 0. \tag{4}$$

This, on integration, yields

$$\frac{\mathrm{d}\theta}{\mathrm{d}t} = \frac{h}{r^2}, \tag{5}$$

where h is the integration constant. After a few mathematical steps, one obtains the following equation

$$\frac{1}{r} = \frac{GM}{h^2} + C\cos(\theta). \tag{6}$$

Let

$$A = GM/h^2. \tag{6a}$$

In Fig. 1, '2a', and '2b' are the major, and minor diameters of the elliptical orbit. The location of the Sun is specified to be at a distance equal to 'c' from the geometrical center of the ellipse, where,

$$c^2 = a^2 - b^2. \tag{6b}$$

Using eqn (6), at $t = 0$ (initial condition on the midnight of December 21), $\theta = \pi$, $r = r1 = a - c$ (Fig. 1).

$$\frac{1}{a-c} = \frac{GM}{h^2} - C, \tag{7}$$

and, when $r = r2 = a + c$, $\theta = 0$, we get

$$\frac{1}{a+c} = \frac{GM}{h^2} + C. \tag{8}$$

Using these two conditions, eqns (7) and (8), we get

$$h = \sqrt{(GM(a^2 - c^2)/a)}. \tag{9}$$

We can define the eccentricity 'e' as

$$e = c/a. \tag{10}$$

From eqn (8), one can obtain

$$C = (1/r_2) - (GM/h^2). \tag{11}$$

One can integrate eqn (5) where r is substituted from eqn (6), and A from eqn (6a). Then, one can get

$$\int_0^{\theta} \frac{\mathrm{d}\theta}{h(A + C\cos(\theta))^2} = \int_0^{t} \mathrm{d}t. \tag{12}$$

Using the integration software 'MAPLE' one obtains

$$t = -2\frac{C\tan\left(\frac{1}{2}\theta\right)}{h(A-C)(A+C)\left(A + A\tan\left(\frac{1}{2}\theta\right)^2 = C\tan\left(\frac{1}{2}\theta\right)^2 + C\right)}$$

$$-2\frac{C\arctan\left(\frac{(A-C)\tan\left(\frac{1}{2}\theta\right)}{\sqrt{(A+C)(A-C)}}\right)}{h(A-C)(A+C)\sqrt{(A+C)(A-C)}} + 2\frac{\arctan\left(\frac{(A-C)\tan\left(\frac{1}{2}\theta\right)}{\sqrt{(A+C)(A-C)}}\right)}{h(A-C)\sqrt{(A+C)(A-C)}}.$$

Equation (13) is a nonlinear (transcendental) equation, and one can solve for θ at any instant. After obtaining θ, one can obtain r using eqn (6). In this way, one can locate the Earth's position at any instant of time.

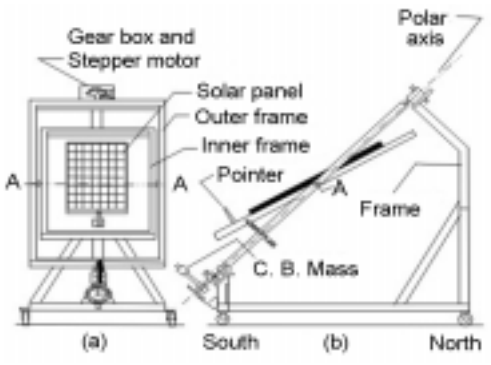

FIG. 2. The solar tracking system.

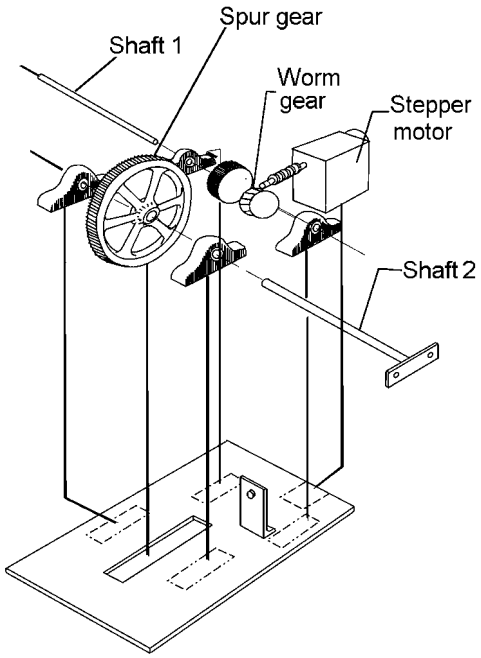

FIG. 3. Gearings in the system.

3.2. *Three-dimensional kinematic equations for tracking the Sun: Use of transformation matrices*

One can track the Sun in such a way that its rays fall perpendicular to the solar panels shown in Fig. 2 which has a gear box whose components are shown in Fig. 3 (A detailed discussion of the construction of the tracking system is presented later.) In this way, one maximizes the incident energy on the panel. This is achieved by defining a series of transformation matrices [17]. A transformation in which there are displacements X1, Y1, Z1 along any set of x-, y-, z-axes, and rotation θ about the z-axis is given by

$$[T_Z] = \begin{bmatrix} \cos\theta & -\sin\theta & 0 & \text{X1} \\ \sin\theta & \cos\theta & 0 & \text{Y1} \\ 0 & 0 & 1 & \text{Z1} \\ 0 & 0 & 0 & 1 \end{bmatrix}. \tag{14}$$

Other transformation matrices about the X-, and Y-axes are given in Appendix A.

One can relate the coordinate systems such as (Xs–Ys–Zs) shown in Fig. 1, and the coordinate system (X9–Y9–Z9) on the solar panel shown in Fig. 4 by the use of the transformation matrices given in Table I. In this table, the first column contains the names of the transformation matrices. The first transformation matrix helps locate a coordinate system at the center of the Earth when it is at A as in Fig. 1. We are measuring this location of the

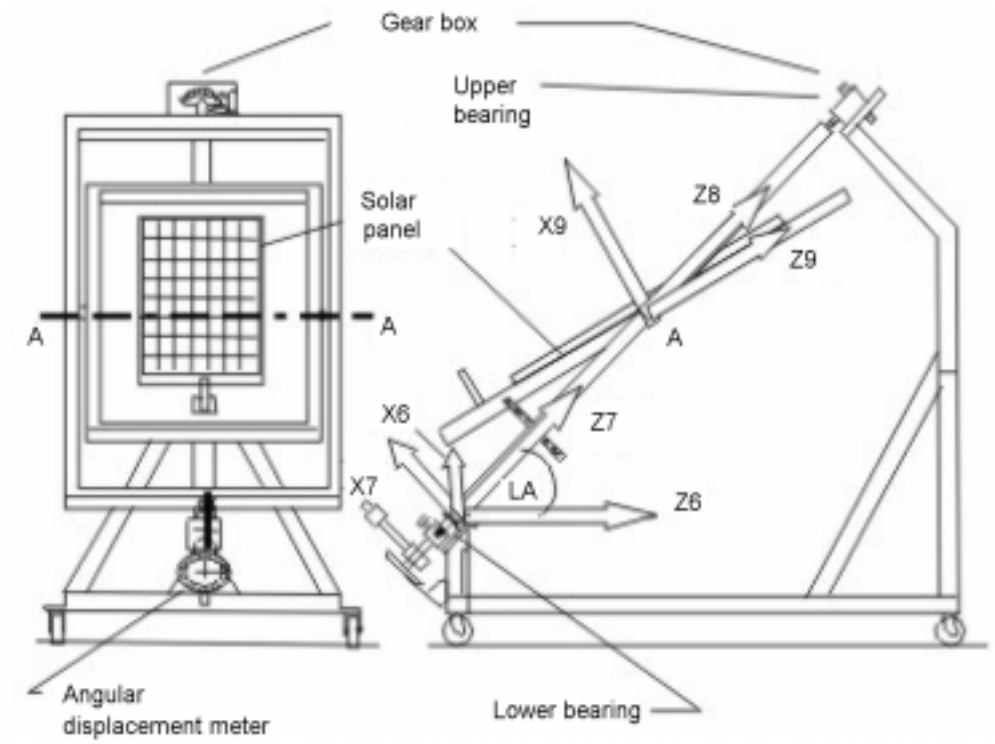

FIG. 4. Various coordinate systems.

Earth in the polar coordinates (r, θ) with the origin at the Sun. In this transformation, there is no rotation about any axis. So, we move from the center of the Sun to the center of the Earth in the Sun's equatorial (ecliptic) plane. It is to be noted that the Earth's axis of rotation is inclined at 23.5° with respect to the normal to the Sun's ecliptic plane. The inclination of this axis remains the same irrespective of the time of the year.

The next transformation [T3] is to rotate about the current Y-axis, which is Y2, by an angle equal to the tilt of the Earth's rotational axis which is 23.5°, and this quantity is represented by TI, in the third column of Table I. By using a series of transformation matrices given in Table I, one can arrive at the origin of the coordinate system X9–Y9–Z9 located on the solar panel (Fig. 4). The details of transformations are given in [18]. A few transformations represented by the letter A are found in Table I. The variables in these are based on design parameters of the tracking system at St John's.

The transformation [A7] involves rotation about the current Y6-axis in the counterclockwise direction (ccw) by an amount equal to the latitude of St John's. Thus, the Z7-axis is parallel to the Earth's rotational axis as shown in Fig 4. In [A8], one translates by L/2 (L is the distance between the upper and lower bearings as shown in Fig. 4) along the Z7-axis to come to the center of the solar panel. Now, we have Y8 as the rotational axis along A–A as shown in Fig. 4. This is for the seasonal variation. The tracking axis is the Z7-axis. This

tracking is done by the stepper motor which rotates the frame assembly about the polar axis (Z7). The matrix for the tracking will be ATR. The rotational rate of the solar panel in Fig. 4 will be equal to that of the Earth but in the opposite direction, i.e. it will be clockwise when viewed from the top.

The matrix [A9] is used to account for the declination of the Sun and its values can be obtained from Kreith and Black [19]. This rotation is given for the seasonal variation. It will be clockwise during March 21–September 21 in the northern hemisphere, and counter-clockwise in the other half of the year.

After defining the above-mentioned transformation matrices, one obtains the following two matrices.

The forward transformation matrix (as seen from the Sun)

$$[TF] = [T12][T3][T4][TEAR][T5][T6][A7][A8][ATR][A9], \text{ and} \tag{15}$$

the inverse transformation matrix (as seen from the solar panel)

$$[TI] = [TF]^{-1}. \tag{16}$$

If we look at the Sun, while standing on the solar panel, the Sun should be along the X9-axis all the time, if the tracking is done correctly (Fig. 4).

Table I
Various transformation matrices

Name	Purpose	Variables	Type	Amount
[T12]	Position of the Earth	r, θ	Displacement	r m, and θ radians
[T3]	Rotation about current Y-axis	TI = 23.5°, the tilt of the Earth's spin axis	Rotation	23.5°
[T4]	Rotation about current Z-axis	LO (Longitude of St John's, Canada)	Rotation	53.25°
[TEAR]	Rotation about current Z-axis	φ (Rotation of the Earth in time t)	Rotation	φ°
[T5]	Rotation about current Y-axis	LA (Latitude of St John's)	Rotation	47.5°
[T6]	Displacement along the current X-axis	R*	Displacement	R* m
[A7]**	Rotation about current Y-axis	LA	Rotation	47.5°
[A8]	Translation along the current Z-axis	L/2	Translation	L/2 m
[ATR]	Rotation about current Z8-axis	$\varphi 1 = -(\varphi - 53.25°)$	Rotation	$\varphi 1$°
[A9]	Rotation about current Y8-axis	δ (Declination)	Rotation, cw during March 21 to Sept. 21; ccw during Sept. 21–March 21	δ°

R = radius of the Earth up to the sea level + the elevation of the tracking system's base above the sea level + h, height of the (X6–Y6–Z6) system above the base (see Fig. 4).
**The transformation matrices have been named T when located inside the Earth or from the Sun to the Earth; they are named A when these are above the Earth.

3.3. *Design of the structure for experimentation*

To verify the theoretical derivations, a solar tracking system was designed, and fabricated to check if the orientation of the solar panel at given time t is normal to the Sun's rays as explained earlier. In the polar mounting of the tracking system, the system's rotational axis is designed parallel to the Earth's spin axis as shown in the side view of Fig. 4. This is achieved by having the base of the system horizontal, and along the geographical north–south line. In the northern hemisphere, the elevation on the north end is higher, whereas in the southern hemisphere, the opposite will be true. To make the rotational axis parallel to that of the Earth, the inclination of the polar axis in Fig. 2 is equal to the latitude of the place of use as shown in Fig. 4. The front view shows two rectangular frames where the inner frame can rotate with respect to the outer frame about the axis A–A (Fig. 5) where the latitude angle is represented by 'LA'. In the detailed construction of the rotating frame assembly shown in Fig. 5, one can see the solar panel mounted on a wooden plank which covers the inner area of the inner frame. The rotation of the inner frame with respect to the outer frame is made possible by the use of two pins. On the other hand, at the two ends of the outer frame are the two other shafts for their support on two bearings. The lower bearing is a tapered roller bearing, and the other can be a ball bearing, although another tapered roller bearing in the reversed position at the upper level will be better.

The rotation about the A–A-axis is of a fixed amount at a given time; it is due to the seasonal variation (declination of the Sun). It can be changed in about 10–15 days. This rotation can be seen in Fig. 4. Here, at point A, one can see two sets of coordinate axes, one mounted on the solar panel called X9–Z9, and the other on to the outer frame (Z8–X8). This tracking motion is provided by a stepper motor–gear box assembly shown in Fig. 3.

In Figs 2 and 4, the area at the base is large. This is desirable because it provides mechanical stability against rigid body rotation of the structure under high wind loads. This problem is similar to those of cars which are supported on four wheels. The wider the car the more stable it is against overturning under high wind loads from the sides. Furthermore, the use of the frames, and small-length shafts at either bearings, takes care of the flexural problems under high wind load conditions.

To minimize the torque needed by the stepper motor, the following points are considered:

(1) It is desirable to have the center of gravity of the combined inner and outer frame assembly at the intersection of the A–A axis and the polar axis (Figs 2 or 4). These two axes ought to be coplanar ideally. This way, the rotational mass moment of inertia is minimized.

(2) Any residual unbalance in the rotational motion due to manufacturing or other errors is taken care of by having a counter-balancing mass as shown in Figs 4 (side view) and 6. In Fig. 6, this mass is located at a radial distance '$r1$' from the axis of rotation, and at an angle from an arbitrarily defined reference line. The best position of this balancing mass is found by moving the position of the mass radically outward–inward from the polar axis (shaft center) where its angular orientation is such that this assembly has no unbalance if rotated around 360°. In other words, one can mass-balance this rotat-

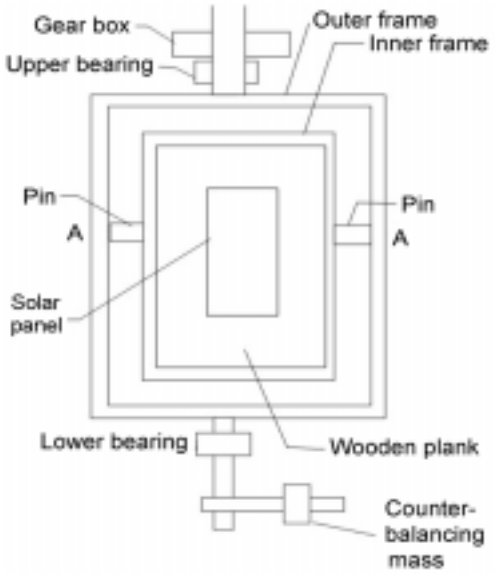

FIG. 5. Frame assembly.

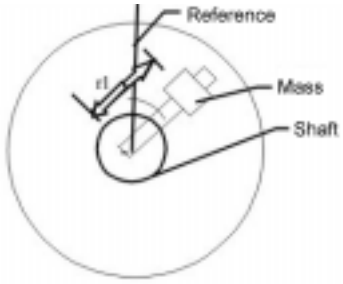

FIG. 6. Mass balancing.

ing frame system by a mass whose position is specified by two degrees of freedom from the polar axis (shaft in Fig. 6). This method of counter-balancing can address any kind of weight distribution of the rotating frame whose center of gravity may or may not lie at the intersection of the two axes (axis A–A, and the polar axis).

4. Automation and tracking

The stepper motor was chosen because of its high torque characteristic at small angular velocities and positioning accuracy [20]. The gear reduction was done in two stages: worm and worm gear with a ratio of 1 to 20, and another spur gear set with a reduction of 15 to 100.

The tracking angular speed was obtained by providing pulses to the stepper motor at the rate of 22.25 Hz. The system was designed to track the Sun during the day between 6 am and 6 pm at the rotational rate of the Earth (this time range is adjustable). At the end of the day, the motion was reversed by providing a limit switch which activated the reverse motion set at four times the tracking speed, which is also adjustable. It took three hours for the tracking system to go back to the starting position. There was another limit switch which stopped the reverse motion and caused a time delay switch to turn on for the balance of the 9 h.

The circuit diagrams for the above-mentioned motions are shown in Figs 7–13. Figure 7 shows the complete diagram which can be divided into five sub-sections where each sub-section is located within dotted line: (1) Timer, (2) Relay, (3) Motor and motor drive circuitry, (4) Divider circuit, and (5) Rotation detection circuitry.

4.1. *Timer*

The combination of R2, R3, and C2 allows for the experimental (by varying R2) setting of the frequency corresponding to the manual speed which is 16 times of the tracking speed

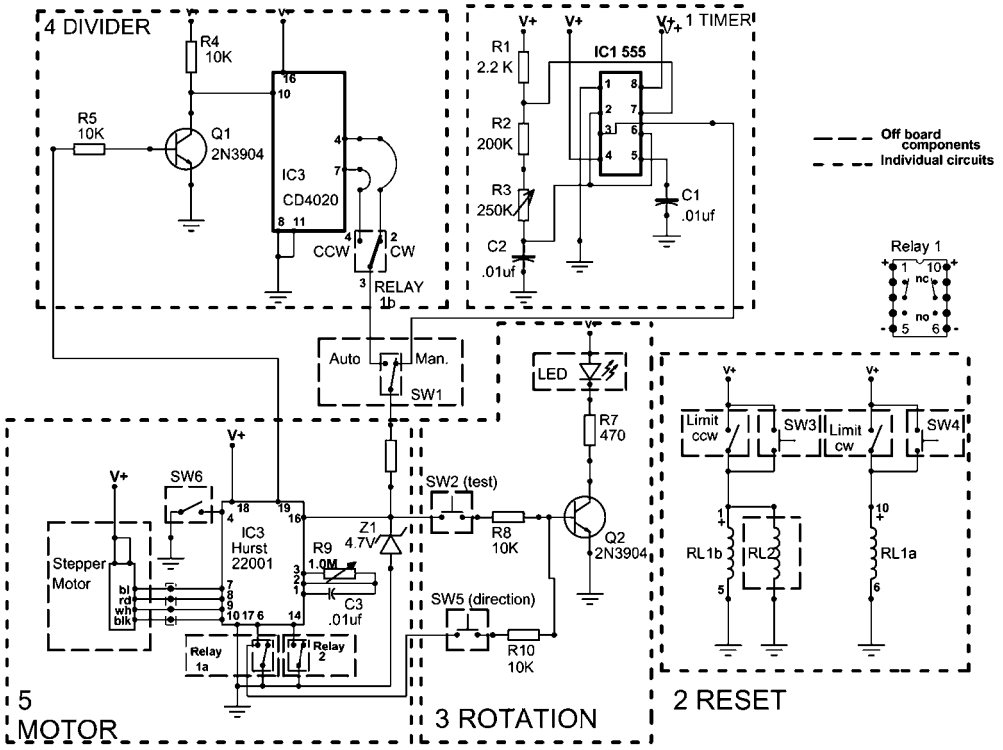

FIG. 7. Complete circuit diagram.

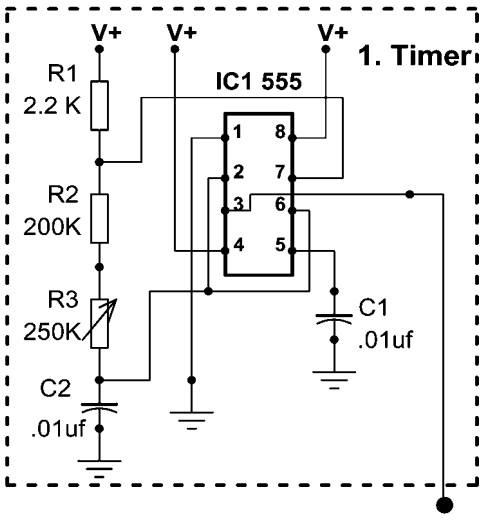

FIG. 8. Timer circuit.

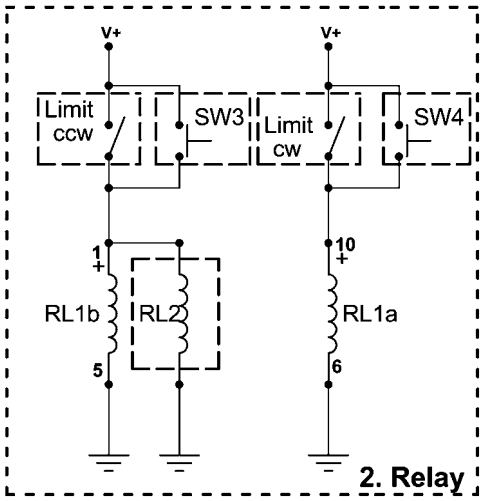

FIG. 9. Relay system.

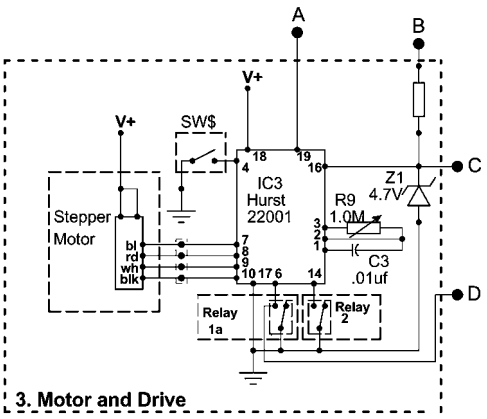

FIG. 10. Motor drive system.

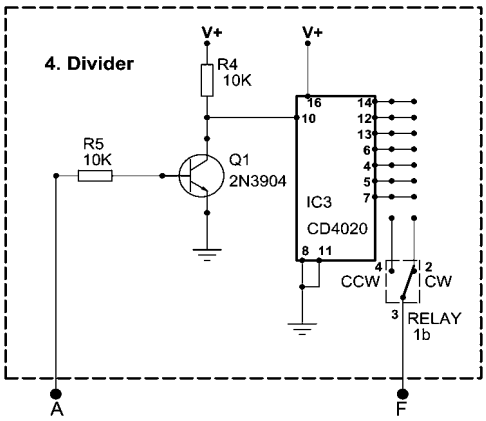

FIG. 11. Divider circuit.

(Figs 7 and 8). R2 allows the unit to be tuned to a required frequency output (16 times the tracking frequency), which is fed to SW1 (Fig. 7). SW1 is the manual/automatic switch. In the manual mode, SW1 feeds this signal to the input of the stepper motor drive chip IC3 (Fig. 7). This is needed to manually turn the motor for setting adjustments, in case of power failures or initial setting. In either of these two cases, the system has to be brought to the correct position, and then set to tracking speed using the auto option available (SW1) (Figs 7 and 13).

4.2. *Relay*

The relay circuit consists of two relays, two switches, and two push-button switches (Figs 7 and 9). Relay 1 is a latching relay. When the limit switch is connected, pin 10 of the relay is activated, and the relay switch is latched on. Relay 1 selects the direction at pin 6 of IC3 (Fig. 7), and Section 2 of Relay 1 selects the output of IC3, i.e. either the tracking speed or four times the tracking speed. This causes the tracking unit to return to waiting for the next morning position. The return speed is four times higher than the tracking speed. Once the unit has returned to waiting for the next morning position, Relay 1 is de-latched; consequently, the direction of rotation is reversed, and also the speed becomes the tracking speed. At the same time, Relay 2 is energized, sending the motor control chip IC3 to the standby state. Relay 2 is the time delay relay; when activated, it takes pin 14 of IC3 low for a predetermined amount of time. Once the time has passed, the relay removes this low, allowing IC3 to function normally. The unit becomes ready to track the Sun again.

4.3. *Motor and drive circuitry*

The stepper motor is driven by Hearst 22001 integrated circuit, and a stepper motor driver IC (Figs 7 and 10). The IC requires a few more components to function. A stream of pulses is fed to pin 16, the input, to cause the motor to rotate. The height of the pulses is kept at 5-V level. This is achieved by using a Zener diode (4.7 V) at the input. The resistor capacitor combination at pins 1, 2 and 3 allows for the setting up of the output in Hz which is quite

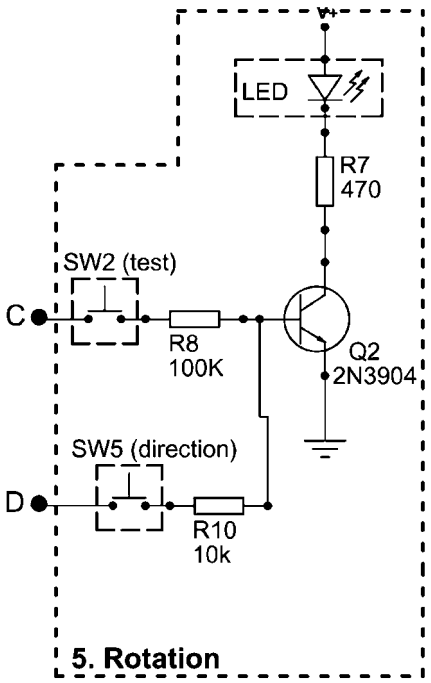

FIG. 12. Rotation detection circuit.

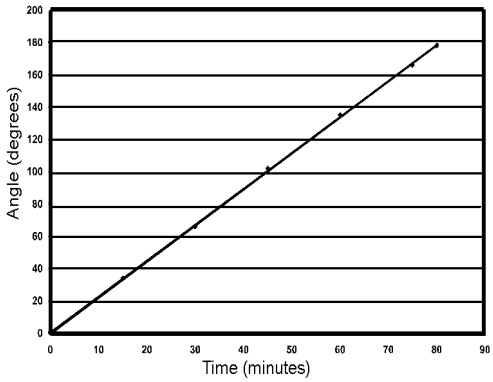

FIG. 14. Variation of angle vs time.

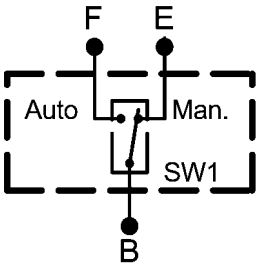

FIG. 13. Manual auto switch.

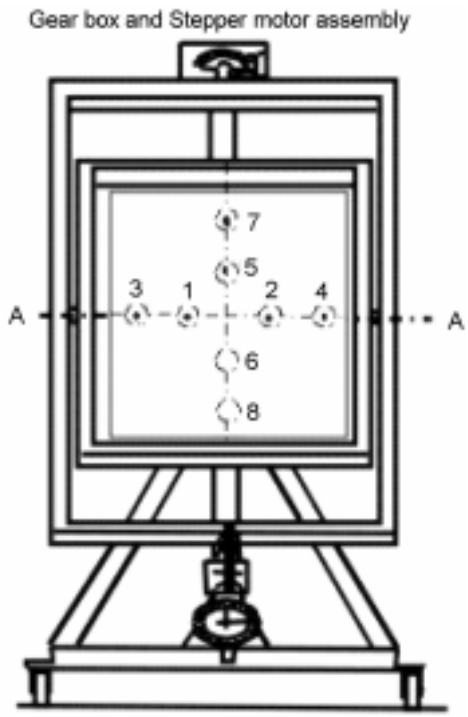

Points	1–2	3–4	5–6	7–8
Distance (cm)	33	66	74	148

FIG. 15. Mass placements.

high (1424 Hz) for the mechanical system under consideration. At this frequency, the selected small horse-power stepper motor will stall due to lack of sufficient power to drive this system at such a high angular speed. It is also not necessary to rotate the panels at such high speeds or frequencies. The system does not need to operate at this frequency due to slow rotational rate of the Earth's axis of rotation. Therefore, this frequency has to be further divided to a slower frequency to match the Earth's rotation rate in the forward motion during the day and the return motion can be several times faster but not 1424 Hz. Later on,

it will be shown that the tracking speed (forward motion) requires the setting at 22.25 Hz, and the return motion can be four times faster than this rate.

This output from the divider can be obtained from pin 19. A high on pin 14 causes the unit to run; pin 6 controls the direction of rotation of the stepper motor. Pin 14 is used to disable the chip (IC3), i.e. it puts the chip on the standby mode, if the signal is at low. The outputs to the motor are on pins 7, 8, 9, and 10. Pin 17 is ground.

4.4. *Divider circuitry*

The divider circuit (Figs 7 and 11) consists of a transistor, and an IC, CD4020. This IC has multiple outputs (divided outputs). The transistor Q1 2N3904 is used to convert the 5-V input signal (pulse) into 12-V signal which is required by CD4020. The output of CD4020 can be over a range 2, 16, 32,…, 16, 384. In the present case, two outputs are provided for. The selection of the speed was determined from the relay circuitry discussed earlier.

In summary, the relay circuitry controlled the (a) direction of rotation on pin 6 in the motor and drive circuitry (IC3), (b) enabling and disabling of it (pin 14), and (c) selection of tracking frequency or four times the tracking frequency in the divider circuitry.

4.5. *Rotation detection circuitry*

This circuitry consists of two switches, three resistors, a transistor, and other related components (Fig. 12). The transistor Q2 2N3904 drives the light-emitting diode (LED). When SW2 (test) is depressed, the LED glows, and at a rate determined by input to IC3, which is 22.25 Hz for the tracking (forward motion) speed. It will flicker at the same frequency as the signal going through SW2. It will be discernible to the eye at 22.25 Hz but almost continuous at four times this frequency (return speed). If there is no signal, then it will not glow. This frequency is further divided mechanically using the gear reduction mentioned earlier. SW5 is used to determine the direction of rotation; when pin 6 (IC3 in Fig. 7) is high (SW5 depressed), LED will not glow, but will glow when SW5 is not depressed. In the latter case, pin 6 is low.

The tracking system was started at 12 noon when the pointer shown in Fig. 4 was aligned with the Sun's rays using the manual speed option. Then, it was set on auto to follow the Sun. It was found that the tracking was accurate. The system tracked the Sun until 6 pm, and returned faster (four times the tracking speed) to the next morning position when the time delay system began operational. The following morning, it started to track the Sun. In this way, it verified the validity of the equations derived in Section 2, and the design of the mechanical structure, and the associated electronic circuitry.

4.6. *Optimal torque testing*

The optimal torque design of the mechanical structure, and the associated electronic circuitry were tested by rotating the panel at the rate corresponding to the frequency of 195.6 Hz at the stepper motor. The angular rotation rate can be obtained from the slope of the graph (Fig. 14).

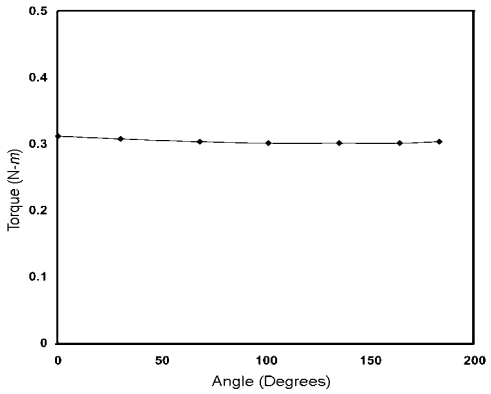

FIG. 16. Torque vs angle.

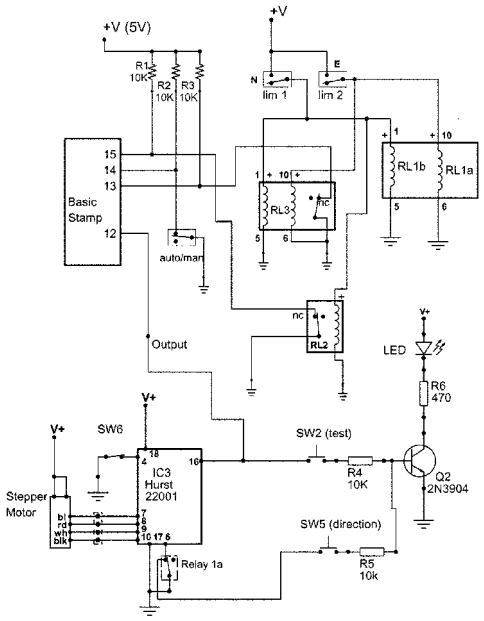

FIG. 17. Day-time tracking.

The stepper motors have their current proportional to the torque. In the experimental set-up shown in Fig. 15, two masses (9.525 kg each) were placed symmetrically about the A-A axis; for example, at points 7 and 8 at a given instant of time (Fig. 15). Similarly, they were placed on positions 3 and 4 also and the torque was tested. If the system is not torque-minimized then there would be a maximum and a minimum torque as the solar panel undergoes rotation. The maximum value would be much more than the torque values shown in Fig. 16. The range shown in Fig. 16 is between 0 and 180° which is sufficient to know the variability of torque. One need not have to go through 360°.

In the present case, a comparatively larger structure was driven by a very small stepper motor. The positional accuracy achievable with such systems is far more than what is possible with photosensor-based dc motor drives where the motion is provided at much coarser time intervals with the possibility of over or undershooting.

To point to any general direction in the three-dimensional space, one needs two orthogonal axes. The tracking system that has been designed here has two orthogonal axes where the polar axis is mass-balanced. Therefore, this system can be used very easily to observe other planets or constellations using larger telescopes.

Furthermore, one can use this system for mounting large paraboloids for concentrating solar energy into a stationary receiver on the ground. In this case, the position of the receiver is fixed to the principal plane of the paraboloid. However, its position is moved towards or away from this paraboloidal mirror when the seasonal variation is given.

Such automated systems go a long way in combating environmental problems by providing clean, and unlimited renewable energy.

5. Accurate tracking using microprocessors

The paper incorporates microprocessors to provide accurate frequency than one generated by the combination of resistors, and capacitors (frequencies generated by an RC circuit). Besides, one needs a system which is (a) cost-effective, (b) widely applicable to both developed and developing countries, (c) accurate with the passage of time as well as with differing temperature conditions such as in deserts or polar regions, (d) easy to operate, and (e) does not require high torque (high horse power motor). The paper deals with a system which satisfies all these requirements unlike any other tracking systems presently in use.

Several research workers [6–8] have used microprocessors to maximize the power output by controlling the operating voltage while others have used for power generation in satellites. The problem solved in the present work is to generate maximum power with minimum energy consumption.

The use of microprocessors here is for (a) generating frequency accurately, and (b) other functions involved in the automatic operation of the system such as selecting the forward or return motion at the correct instant of time.

5.1. *Tracking using a timer*

The stepper motor was chosen because of its high torque characteristic and positioning accuracy (Fig. 4). Such a motor is widely used in robotics for this reason. In the tracking process (Fig. 17), pulses are sent from the microprocessor at 22.12 Hz (measured) where the step angle of the motor is 0.025°. The gear reduction is done in two stages: (1) worm and worm gear with a ratio of 1 to 20, and another spur gear set with a reduction of 15 to 100 (Fig. 3). Thus, the accuracy of the system (panel rotational accuracy) is equal to $0.025 \times (1/20) \times (15/100) = 1.875 \times 10^{-4}$ degrees. Such an order of accuracy for a given cost is not possible in any other systems, thermal or photosensor based. These sensors are located at certain angular intervals which are placed at much larger angular intervals than 1.875×10^{-4} degrees. Theoretically, the motions are intermittent in both these cases. If a synchronous gear motor is used then it would require large gear reduction because the Earth's rotation rate is extremely slow. There are several disadvantages in such cases. In that event (a) the rotational dynamic inertia will increase requiring greater horse-power motor, (b) the frictional losses will increase, (c) greater volume space will be required, and (d) the cost due to several gears will also increase. On the other hand, the disadvantage is that if the stepper motor misses some pulses then inaccuracy can creep in the absence of any feedback control. Secondly, a problem will persist if there is initial error in the start up.

Stepper motors have found application in numerical control machines (lathes, milling machines), etc. Their use is time-tested and is found to be quite reliable.

The tracking angular speed is obtained by providing pulses to the stepper motor at the rate of 22.12 Hz. The system can be designed to track the Sun during the day starting at 6 am until 6 pm at the rotational rate of the Earth. At the end of the day, the motion was reversed by providing a limit switch which activated the reverse motion set at four times the

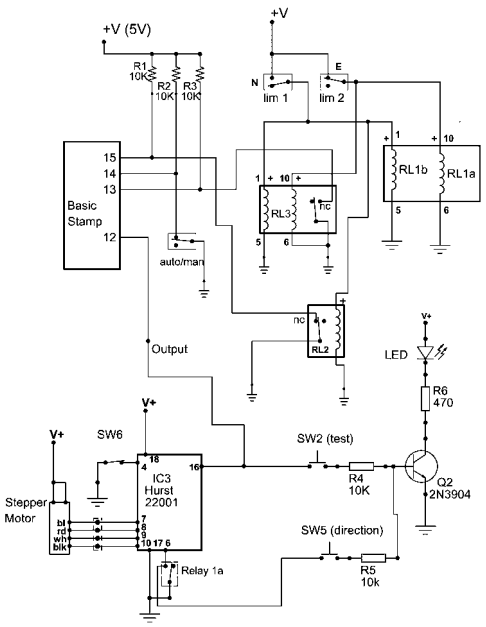

FIG. 18. Evening return.

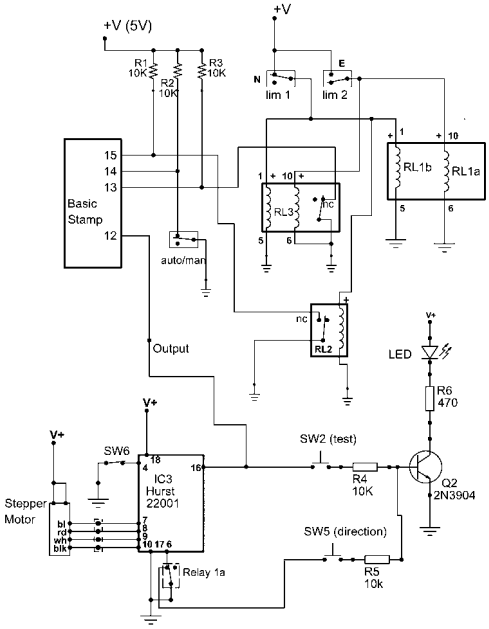

FIG. 19. Morning position (waiting).

tracking speed. It took three hours for the tracking system to go back to the starting position (the morning position). There was another limit switch which stopped the reverse motion and caused a time delay switch to turn on for the balance of the nine hours. The circuit diagrams for these motions are shown in Figs 17–19. Appendix B provides detailed description.

It should be pointed out here that the range of angular displacement for the daily motion as set by the two limit switches can be varied. In summer months, this range can be longer compared to that in winter. The waiting time settings in the timer, in this case, have to be adjusted accordingly.

5.2. *Precision tracking*

Figure 1 shows the Earth's orbit around the Sun where the Sun is located at the focus of the elliptical path of the Earth. One can see that the Earth's spin axis makes an angle equal to 23.5° from the normal to the plane of orbital motion. The result is that the Sun, as seen from the Earth, does not move with a uniform angular velocity. There are several causes for this, the first one being the inclination of the Earth's spin axis, and the second, the elliptical path, causes radial, and angular accelerations. The third reason for the nonuniform motion can be understood from Fig. 20 where one sees the change in the orientation of the Earth's spin axis on a conical surface. The axis of the conical symmetry is normal to the plane of ecliptic (the plane containing the Earth's orbital trajectory). This is due to the pull of the moon and other planets such as Jupiter. In this figure one also sees the couple which acts as the righting couple (to counter the gravitational pulls) to bring the spin axis normal to the plane of the Earth's orbital motion.

To track accurately, one also needs to know the equation of time which can be understood as the difference, over the course of a year, between time as read from a sundial and a clock. It varies from day to day in a given year. For example, it can be ahead by as much as 16 min, and 33 s or fall behind by as much as 14 min, and 6 s. It results from an apparent irregular movement of the Sun caused by a combination of the obliquity of the Earth's rotation axis, the eccentricity of its orbit, etc.

A plot of equation of time vs the day of the year (the year 2000) is shown in Fig. 21. It shows the error between a normal clock, and the time given by a sundial. For discussion about various causes of errors in time one can refer to [21–24]. The tracking of the Sun is an inverse problem where one computes the clock time based on the observations on a sundial. The necessary equations for this are given by:

$$\text{Equation of time (ET)} + \text{Clock time (CT)} = \text{Sundial time (Alignment of the pointer of the solar panel with the Sun's rays)} \quad (17)$$

$$\text{Alarm time (AT)} = \text{Equation of time (ET)} + \text{Clock time (CT)} \quad (18)$$

Hence, to track the Sun accurately, one has to start the tracking process by setting an alarm by taking into account the ET, during any day of the year. Here, the motion starts at the alarm time set in the microprocessor program.

There are two options available here. In the first, one can equate ET to zero, and start at the same clock time. Of course, in this case, the Sun rays would not be normal to the panels because ET has significant value at different days of the year. In the second, one can store the various ET values in the memory of the microprocessor, and on the corresponding days, the microprocessor retrieves the correct value from its memory, and starts the motion at the correct instant of time by adding ET to the clock time.

The experiments can be carried out by modifying the electronic circuit shown in Figs 17–19. The new circuit with the real-time clock is shown in Fig. 22. The associated computer program is also written. In Fig. 22, the real-time clock is connected to the basic stamp microprocessor. In the computer program, the cycle (the tracking motion) starts if the specified time (alarm time) in the clock on a given date is equal to the time displayed in the microprocessor program. This time to start is based on eqn (17). In this figure, one can notice that there is no time-delay system. The ability to change the starting times on different mornings, differentiates a real-time clock from a time-delay relay. This (varied starting times) is not possible to achieve with the time-delay relay system. Secondly, in the case of power failure for some time during the night, it would be a very cumbersome to adjust the time delay again. In that case one would have to reduce the set time in the relay by an amount equal to the duration of the power failure. Thirdly, the cost of the real-time clock is much less than such relays, and fourthly, the accuracy of setting the delay time is much more than what is possible with the relays. The errors introduced every day in such relays do not build up in the case of alarm-activated microprocessor systems. Here, the possible errors introduced by the timer are eliminated, and hence the accuracy of the system is enhanced.

The advantage of this system having corrections for the equation of time over the photosensor-based system is that the present one is entirely based on the motion of the Earth

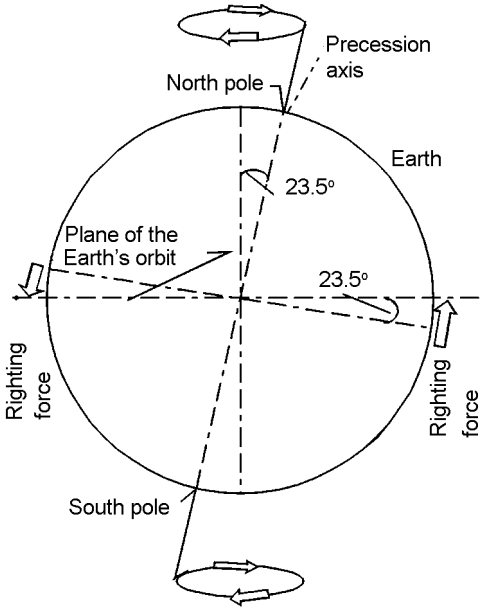

FIG. 20. Precession of Earth's axis.

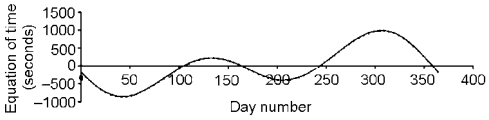

FIG. 21. Variation of equation of time vs day number starting January 1, 2000.

which is very precise, and not dependent on local weather or atmospheric (moisture, dust, etc.) conditions. This system can be widely used in any part of the world. Photosensor-based systems have not found applicability in many parts of the world where dust is very common. The underdeveloped places in the world lack the support system for a sophisticated feedback technology. Moreover, the present system is cheaper to use as compared to any other, such as a dc motor driven with a feedback or a synchronous gear-motor drive.

5.3. *Intelligent tracking after power failures or interruptions*

Figure 23 shows the circuit diagram of a system where the tracking motion is provided by a separate battery. This way one would avoid problems of insufficient battery charge if cloudy conditions prevail over several days.

It is better to safeguard the tracking process due to power failure. To illustrate the concept, let us take an example where the power fails for 'T' seconds. Instead of repositioning the solar panel at the correct angular orientation manually in such cases, ideally one would want the machine itself to properly align itself. In this case, we need a means to detect the time interval of the power failure. In this regard, a microprocessor with a real-time clock provides the means to detect this problem. One can use one of the many pins as an input pin where the voltage becomes low when the power fails.

For this, one needs to record the time of power failure by reading the clock as discussed earlier. The microprocessor keeps checking the condition (low voltage) of this particular pin. When the power is restored this pin gets to the 'high' state. At this moment, the process-

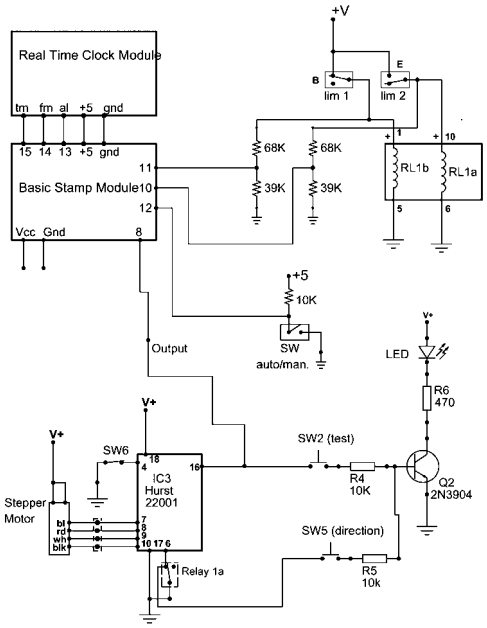

FIG. 22. Circuit diagram with alarm clock.

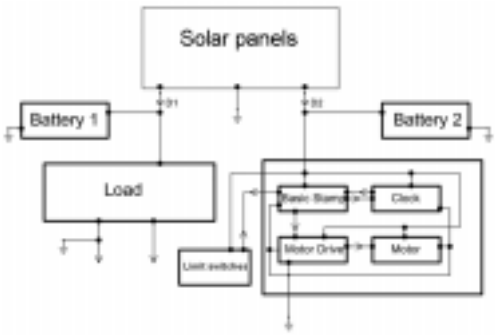

FIG. 23. Block diagram for separate battery compartments.

sor looks at the clock again. Then, it calculates the difference of these two times, and converts it into seconds. This gives the total time when the power is off (say, equal to T seconds).

The realignment to the correct position of the solar panel can be done by calculating the number of pulses that should have been given to the motor in time T. For the system discussed in Section 2.1, the rate at which the pulses are given is 22.12 Hz. Multiplying this frequency by T gives us the total missing pulses during time T.

Next, while these pulses will be provided to change the angular orientation of the panel, some more time will lapse, and consequently, one would need to provide additional pulses to accommodate this additional time period, 'T1'. Since the motor speed in the return motion (faster catching up speed) is four times the speed of the forward motion (tracking motion), T1 is equal to T/4. Thus, the total time for correct alignment with rapid motion would be equal to $T2 = T + (T/4) = (5/4)T$. The corresponding number of pulses for correct alignment would be equal to $N = T2 \times 22.12$.

In the circuit shown in Fig. 24, one can see relay RL 2, when not energized, make the pin 9 'low'. In this condition, switch SW7 is in the 'off' position, and the power supply to the stepper motor is disconnected. When the microprocessor detects this condition, it notes down the time of the clock. When the switch SW7 is in the 'on' position after some time, pin 9 becomes high because relay RL 2 is energized. The microprocessor monitors the clock again, and calculates the number of pulses (N) required and provides these pulses with faster speed, and the normal tracking starts again.

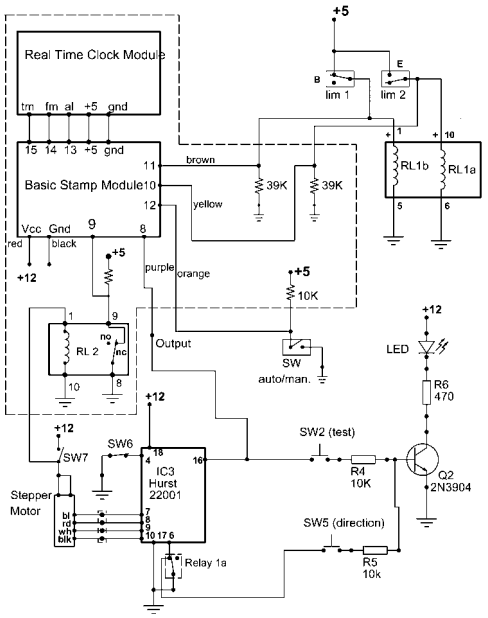

FIG. 24. Circuit diagram for intelligent tracking.

6. Conclusion

In this work, at first, the equations of motion for the Earth were derived. It was followed by another set of three-dimensional kinematic equations for tracking the Sun using the 4×4 homogeneous transformation matrices. To verify the theoretical equations derived (Sun's position and orientation as a function of time), a mechanical system was designed along with electronic circuitry for tracking and automation. The validity of the theoretical equations derived was experimentally verified by checking the correctness of tracking.

In the design of structure, special care was taken to minimize the torque, and hence the horse-power requirements of the motor. Here, it satisfied the condition that the center of gravity of the rotating mass be on the Polar (rotational) axis. Another feature of the design is to have this center to be on the seasonal variation axis so that the system need not be balanced whenever this variation takes place. This design requirement led this center to be located at the intersection of the two axes.

The process also included the design of electronic circuitry for the tracking and automation operation using a microprocessor–time delay combination, and microprocessor–real-time clock combination. The tracking system so arrived at was accurate and inexpensive in comparison to other systems requiring sensor-based feedback.

The system was tested on different occasions in differing seasons, and was found to perform very satisfactorily. In all the cases, there was no shadow cast by the pointer mounted on the frame containing the solar panel.

Acknowledgments

The authors wish to thank the Technical Services of the Memorial University of Newfoundland, Canada, for assistance in the fabrication of the tracking system. They also wish to

thank the Natural Sciences and Engineering Research Council (NSERC), Canada, for financial grant to carry out this research work.

References

1. R. A. Bentley, Global oil depletion–Methodologies and results, *Proc. 3rd Int. Workshop on Oil and Gas Depletion*, Berlin, Germany, pp. 25–26 (2004).
2. T. Hiyama, S. Kouzuma, and T. Imakubo, Identification of optimal operating point of PV modules using neural network for real time maximum power tracking control, *IEEE Trans. Energy Conversion*, **10**, 360–367 (1995).
3. K. Farber, C. A. Morrison, and H. A. Ingely, A self-contained tracking system, *ASME Paper No. 76*, WA/HT-26, Dec. 1996.
4. A. Baz, A. Sabry, A. Mobarak, and S. Morcos, On the tracking error of a self-contained solar tracking system, *Trans. ASME, J. Solar Energy Engng*, **106**, 416–422 (1984).
5. P. T. Huynh, and B. H. Cho, Design and analysis of a regulated peak-power tracking system, *IEEE Trans. Aerospace Electronic Systems*, **35**, 84–92 (1999).
6. P. Huynh, and B. H. Cho, Design and analysis of a microprocessor-controlled peak-power tracking system, *IEEE Trans. Aerospace Electronic Systems*, **32**, 182–190 (1996).
7. K. Ro, and S. Rahman, Two-loop controller for maximizing performance of a grid-connected photovoltaic-fuel cell hybrid power plant, *IEEE Trans. Energy Conversion*, **13**, 276–281 (1998).
8. T. Hiyama, S. Kouzuma, T. Imakubo, and T. H. Ortmeyer, Evaluation of neural network based real time maximum power tracking controller for PV system, *IEEE Trans. Energy Conversion*, **10**, 543–548 (1995).
9. P. A. Davies, Sun tracking mechanism using equatorial and ecliptic axes, *Solar Energy*, **50**, 487–489 (1993).
10. A. B. Maish, Performance of a self-aligning solar array tracking controller, *21st IEEE Photovoltaic Conf.*, Kissimimee, Florida, USA, pp. 864–869 (1990).
11. K. H. Hussein, I. Muta, T. Hoshino, and M. Osakada, Maximum photoelectric power tracking: An algorithm for rapidly changing atmospheric conditions, *IEE Proc. Generation, Transmission Distribution*, **142**, 59–64 (1995).
12. R. Kohne, and M. Simon, Solar concentrators in thermal power plants, *Proc. on Workshop Engineering Aspects of Solar Energy Utilization*, University of Stuttgart, West Germany, April 1977.
13. K. Siri, V. A. Caliskan, and C. Q. Lee, Peak power tracking in parallel connected convertors, *IEE Proc. G, Circuits, Devices Systems*, **140**, 106–116 (1993).
14. S. Agarwal, and A. M. Sharan, *Solar incidence and the orientation of the solar panel*, Research Report, Faculty of Engineering, Memorial University, St John's, Newfoundland, Canada (1994).
15. A. F. D'Souza, and V. K. Garg, *Advanced dynamics*, Prentice-Hall, pp. 67–68 (1984).
16. R. C. Hibbeler, *Engineering mechanics*, MacMillan, pp. 126–132 (1992).
17. J. J. Craig, *Introduction to robotics: Mechanics and control*, Addison Wesley, Ch. 2 (1989).
18. Anand M. Sharan, and M. Prateek, *Use of transformation matrices in derivations of solar tracking systems*, Research Report, Faculty of Engineering, Memorial University of Newfoundland, St John's, Canada (2000).
19. F. Kreith, and W. Z. Black, *Basic heat transfer*, Harper and Row, Ch. 6 (1980).
20. R. D. Klafter, T. A. Chmielewski, and M. Negin, *Robotic engineering—An integrated approach*, Prentice-Hall of India, p. 249 (1994).
21. G. O. Abell, *Exploration of the universe*, Holt, Reinhart, and Winston, pp. 135–137 (1975).
22. F. W. Cousins, *Sundials*, Pica Press, pp. 70–82 (1970).
23. F. W. Cousins, *The solar system*, John Baker, Ch. 3 (1972).
24. G. R. Kaye, *A guide to the old observatories at Delhi, Jaipur, Ujjain, and Benaras*, Academic Press, Gurgaon, Haryana, India, Chs 1 to 4 (1985).

Nomenclature

a = Half of the major diameter of the Earth's orbit
b = Half of the minor diameter of the Earth's orbit
c = A constant
h = A constant
m = Mass of the Earth
r = Distance of the Earth from the origin at the Sun
$r1$ = Distance of the Earth from the Sun on December 21 at midnight
$r2$ = Distance of the Earth from the Sun on June 21 at midnight
$\dot{r}$ = First time derivative of r
$\ddot{r}$ = Second time derivative of r
t = Time
A = A constant
B = A constant
C = A constant
F_r = The radial force on the Earth
F_θ = The force along the θ direction
M = The mass of the Sun
R = The radius of the Earth
[ ] = A matrix
[TF] = Forward transformation matrix from the center of the Sun to the solar panel
[TI] = Inverse transformation matrix from the solar panel to the Sun.
θ = Angular displacement coordinate
· = Time derivative

Appendix A

The transformation matrices about the x- and y-axes are:

$$[Tx] = \begin{bmatrix} 1 & 0 & 0 & X1 \\ 0 & \cos\theta & -\sin\theta & Y1 \\ 0 & \sin\theta & \cos\theta & Z1 \\ 0 & 0 & 0 & 1 \end{bmatrix} \tag{A1}$$

and

$$[Ty] = \begin{bmatrix} \cos\theta & 0 & \sin\theta & X1 \\ 0 & 1 & 0 & Y1 \\ -\sin\theta & 0 & \cos\theta & Z1 \\ 0 & 0 & 0 & 1 \end{bmatrix} \tag{A2}$$

Appendix B

If we look at Fig. 17, we see that it has a motor driver chip (IC3, Hurst 22001), and three relays: (a) RL 1b, and 1a, (b) RL2, and (c) RL3. Each of the coils of RL1 is connected to

the limit switches corresponding to the morning and evening positions. The microprocessor named as basic stamp has pins 13, 14, and 15 connected to the relays discussed earlier. It generates the required frequencies based on the program written for this purpose, and sends them through pin 12. The actual frequencies would be slightly different from those seen in the program because it takes finite but infinitesimal time to execute a given line in the program. One has to experiment, i.e. actually measure the frequencies generated by varying the pause duration in the program. During the day time, the frequency sent is equal to 22.12 Hz. By pressing SW2 switch in Fig. 17, one can check the status or the frequency of the signal by observing the flickering of light in LED. The direction of rotation, whether clockwise or counter-clockwise, can be checked by pressing switch SW5. Pin 6 of the motor driver chip is low when the motor rotation is counter-clockwise. There is another switch which enables one to operate manually if desired and its manual operation provision has to be there in the computer program. In this case, the manual speed would be much faster than the tracking or the return speed. Pins 7, 8, 9, and 10 connect the motor coils. The stepper motor is operated on 12 V.

After the day's travel, limit switch 2 is activated at 6 pm, which results in making pin 13 high (Fig. 18). The frequency is equal to four times the day frequency. The direction of motor rotation is reversed by making the pin of the motor driver chip high. This process is continued until limit switch 1 is contacted. This results into reversing the direction of motor rotation (pin 6-motor driver chip) becoming low again. At the same time, time-delay relay 2 causes pin 15 of the microprocessor to become high. Under this condition, the computer program has to have HOLD which means that the microprocessor stops generating frequencies. Relay 2 is timed for the balance of the 24 h. It reactivates the system by making pin 15 low at 6 am on the following morning. Figure 19 shows the morning position.